UDC 519.6+51-74::628.395

NUMERICAL MODELING OF FILTRATION AND TRANSPORT PROCESSES IN A CYLINDRICAL POROUS FILTER USING THE FINITE VOLUME METHOD

Ravshanov N., *Boborahimov B.I., Berdiyorov Sh.Sh.

*uzbekpy@gmail.com

Digital Technologies and Artificial Intelligence Development Research Institute,
17A, Buz-2, Tashkent, 100125 Uzbekistan.

This paper explores the numerical modeling of flow during filtration and transport of dissolved components in a cylindrical porous medium. The mathematical formulation is based on the axisymmetric Brinkman-Darcy equations describing hydrodynamic processes, as well as a system of equations for convective-diffusion transport taking into account adsorption on a solid matrix. The permeability of the porous medium is specified using the Kozeny-Carman model. The numerical solution is implemented using the finite volume method, which guarantees the fulfillment of conservation laws in each control volume. A computational algorithm for determining the distributions of pressure, velocities, and component concentrations is developed. The influence of porous structure parameters and adsorption kinetics characteristics on the efficiency and characteristics of the filtration process is studied.

Keywords: cylindrical porous medium, filtration, substance transport, Brinkman–Darcy model, adsorption, finite volume method, numerical simulation.

Citation: Ravshanov N., Boborahimov B.I., Berdiyorov Sh.Sh. 2026. Numerical modeling of filtration and transport processes in a cylindrical porous filter using the finite volume method. *Problems of Computational and Applied Mathematics.* 1(71): 28-42.

DOI: https://doi.org/10.71310/pcam.1_71.2026.03

1 Introduction

Filtration and transport of dissolved components in porous media are fundamental to a wide range of engineering and natural systems, including water treatment plants, catalytic reactors, and subsurface hydrogeological processes. The efficiency of such systems is determined not only by the hydrodynamic flow parameters but also by the characteristics of mass transfer and the interaction of substances with the solid matrix of the porous medium. Darcy's law is traditionally used to describe fluid flow in porous media; however, its applicability is limited to cases where viscous effects and boundary layers near the walls can be neglected. In the presence of finite permeability and a significant influence of viscosity, the Brinkman-Darcy model, which takes into account both the resistance of the porous structure and the diffusion of momentum, is more appropriate.

Modeling the transport of dissolved components in porous filters is typically based on convective-diffusion transport equations with additional source terms accounting for chemical reactions and adsorption on the solid phase. Accounting for adsorption processes is fundamental when assessing filtration efficiency, as they determine the filter saturation kinetics and the level of flow purification. Despite the significant amount of research devoted to filtration and mass transfer problems in porous media, the problem of coupled numerical modeling of hydrodynamics and adsorption transport in an axisymmetric cylindrical formulation remains relevant, particularly in terms of developing robust and conservative numerical methods.

The aim of this work is to develop and numerically implement a mathematical model of filtration flow and transport of dissolved substances in a cylindrical porous medium based on the Brinkman–Darcy equations using the finite volume method, as well as to study the influence of porous structure parameters and adsorption kinetics characteristics on the main indicators of the filtration process.

In [1] study investigates unsteady filtration in a sandwich-type reservoir system, which is relevant for layered soils common in Uzbekistan. The model is formulated using parabolic PDEs with boundary conditions and solved analytically via the Laplace transform. Numerical results show that pressure in both layers increases exponentially, while interlayer flow strongly depends on piezoconductivity and filtration coefficients. A generalized formula for well gallery control is also derived for drainage design.

Studies [2, 3] develop mathematical and numerical models for filtration in porous media with coupled hydrodynamics and mass transport. The models account for key mechanisms such as concentration variation, adsorption, cake formation, and pore clogging, which lead to porosity reduction and pressure growth. Numerical simulations show that parameters like barodiffusion, filter thickness, permeability–porosity relations, and initial flow rate strongly affect filtration efficiency and filter lifetime. The proposed stable finite-difference algorithms enable prediction and optimization of filtration performance.

A significant number of works are devoted to the study of flow and transport in porous bodies with different geometries and permeabilities. In particular, in [4], a numerical study of flow past a porous cylinder and the transport of dissolved substances at different Reynolds and Darcy numbers was performed, where the influence of permeability on the flow structure and the formation of a concentration plume was analyzed in detail. The development of computational tools for modeling flows in porous media is presented in [5], where a universal solver based on OpenFOAM is proposed, taking into account phase transformations and additional resistances of the porous structure. A separate area of research is associated with the mathematical modeling of heat and mass transfer and phase processes in porous materials. In [6, 7], microscopic and macroscopic approaches to the description of transport processes are considered, and the features of boundary conditions and the effects of porosity heterogeneity are discussed. In [8], a detailed CFD–DEM model of filtration with the formation of a filter cake is developed, allowing for the interaction of particles, liquid and the filter medium.

Modeling of multiphase flows and transport in porous media is presented in [9, 10], where control-volume numerical schemes and hybrid approaches combining continuum and network models of pore space are used. In [11], the interaction of a flow with a thin elastic porous layer is considered based on homogenization methods, which is important for the correct description of interface effects. Modern research is also aimed at constructing computational models that take into account the complex microstructure of a porous medium and the transitions between Darcy and non-Darcy flow regimes [12]. In [13, 14], mathematical models of membrane filtration are proposed taking into account adsorption, pore clogging, and elastic deformation of pore walls, which allows for the analysis of permeability degradation and the service life of filters.

A separate class of problems is associated with the combined consideration of mass transfer, heat transfer, and additional physical effects such as magnetic fields and local thermal non-equilibrium [15], as well as filtration processes in cylindrical porous regions based on Darcy's law [16]. Biomedical applications, in particular modeling of fluid transport in lymph nodes, are considered in [17], where the porous structure plays a key role in flow regulation. In [18], a detailed analysis of unsteady flow in porous media is carried

out based on averaging the Navier–Stokes equations, which expands the applicability of Darcy- and Brinkman-type models. Thus, despite a significant number of studies, the problem of combined numerical modeling of filtration flow and solute transport taking into account adsorption in an axisymmetric cylindrical porous medium remains relevant, especially in the context of developing conservative and robust numerical algorithms.

2 Problem formulation

Below are the equations for a cylindrical porous filter.

Equations for hydraulics (Brinkman-Darcy):

$$\nabla \cdot \mathbf{u} = 0 \Rightarrow \frac{1}{r}\frac{\partial (r u_r)}{\partial r} + \frac{\partial u_z}{\partial z} = 0. \tag{1}$$

Where: r – radial coordinate[m], distance from the center to the wall, z – vertical coordinate [m], direction from top to bottom, u_r – radial velocity component [m/s], u_z – vertical velocity component [m/s], angular coordinate is zero due to symmetry.

This equation expresses the equation of conservation of mass - the incompressibility of water. This ensures constant equilibrium between the incoming and outgoing flow volumes and guarantees mass conservation regardless of the pressure inside the filter

$$\begin{cases} -\dfrac{\mu}{\varkappa(\varepsilon)} u_r + \mu \nabla^2 u_r - \dfrac{\partial p}{\partial r} = 0, \\ \nabla^2 u_r = \dfrac{1}{r}\dfrac{\partial}{\partial r}\left(r \dfrac{\partial u_r}{\partial r} \right) + \dfrac{\partial^2 u_r}{\partial z^2} - \dfrac{u_r}{r^2}. \end{cases} \tag{2}$$

Where: μ – dynamic viscosity [Pa·s], for water 0.001 (20 ∘C da), $\varkappa(\varepsilon)$ – permeability [m^2], flow capacity, p – pressure [Pa].

This equation is the radial momentum equation, which governs the radial velocity with the pressure gradient and pore resistance. If the pressure differs from the center to the wall, the fluid flows radially, but pore resistance slows down this movement.

$$\begin{cases} -\dfrac{\mu}{\varkappa(\varepsilon)} u_z + \mu \nabla^2 u_z - \dfrac{\partial p}{\partial z} = 0, \\ \nabla^2 u_z = \dfrac{1}{r}\dfrac{\partial}{\partial r}\left(r \dfrac{\partial u_z}{\partial r} \right) + \dfrac{\partial^2 u_z}{\partial z^2}. \end{cases} \tag{3}$$

This equation drives the flow with the pressure difference for the axial momentum equation - the main direction of the flow (from top to bottom). Porous resistance and viscosity slow down the flow. Therefore, the flow rate at the outlet changes depending on the pressure difference.

$$\varkappa(\varepsilon) = \frac{\varepsilon^3 d_f^2}{180(1-\varepsilon)^2}. \tag{4}$$

Where: ε – porosity, $(0 < \varepsilon < 1)$, proportion of free space, d_f – filter particle diameter [m].

This equation expresses the Kozeny-Carman formula and relates the internal structure (porosity) of the filter to the flow capacity. In a coarse-grained or more porous filter, the flow passes more easily.

The general equation for the change in pressure for a cylindrical coordinate system:

$$\varepsilon\beta \frac{\partial p}{\partial t} = \frac{\varkappa(\varepsilon)}{\mu}\left(\frac{\partial^2 p}{\partial r^2} + \frac{\partial^2 p}{\partial z^2} - \rho g \frac{\partial p}{\partial z} \right). \tag{5}$$

where β – fluid compressibility[1/Pa].

For substance transport (for each $i = 1, \ldots, N$), the following equations (6) – (9) are expressed:

$$\begin{cases} \dfrac{\partial (\varepsilon c_i)}{\partial t} + \nabla \cdot (u c_i) = \nabla \cdot (\varepsilon D_i \nabla c_i) - R_i, \\ R_i = r_i^{bulk} + a_s r_i^{surf}. \end{cases} \tag{6}$$

Here: t – time [s], for the dynamics of the process, N – number of components, c_i – concentration of the i-th component in water [mol/m^3 or kg/m^3], $D_{i,\text{eff}}$ – effective diffusion coefficient [m^2/s], $r_{i,\text{bulk}}$ – bulk reaction rate in solution [mol/(m^3·s)], a_s – surpace area of per unit volume [m^2/m^3], $r_{i,\text{surf}}$ – surface loss rate [mol/(m^2·s)].

This equation is called the ADR (advection-diffusion-reaction) equation and shows how the concentration of each harmful substance in water changes: change over time = flow transfer + diffusion - reaction - adsorption. This allows you to calculate the quality of the water exiting the filter.

$$\frac{\partial q_i}{\partial t} = k_{f,i}(q_i^* - q_i). \tag{7}$$

Where: q_i – capture quantity in the solid phase $[mol/kg]$, $k_{f,i}$ – LDF(linear driving force) kinetic coefficient [1/s], q_i^* – equilibrium adsorption quantity [mol/kg].

This equation represents the adsorption kinetics (LDF) equation and tells us at what rate harmful substances are absorbed into the filter particles. If the particle is still free, a large amount of harmful substance is absorbed; if saturated, absorption slows down

$$q_i^* = \frac{q_{i,\max} b_i c_i}{1 + \sum_{j=1}^{N} b_j c_j}. \tag{8}$$

Where: $q_{i,\max}$ – maximum adsorption capacity [mol/kg], b_i – Langmuir affinity coefficient [m^3/mol].

This equation represents the Langmuir isotherm. In this case, due to the limited surface area of the adsorbent, harmful substances compete for space and explain the decrease in the efficiency of the filter over time:

$$r_{i,surf} = \rho_s \frac{\partial q_i}{\partial t}. \tag{9}$$

Where: ρ_s – density of adsorbent particles [kg/m^3].

This equation expresses the rate of surface loss. In this case, the change in adsorption in the solid phase reduces the concentration in the liquid. This links the mechanism of loss of harmful substances to the liquid and solid phase.

The colmatation (optional, particle) equations (10)-(11) defined as follows:

$$\frac{\partial (\varepsilon c_p)}{\partial t} + \frac{1}{r}\frac{\partial}{\partial r}(r c_p u_r) + \frac{\partial}{\partial z}(c_p u_z) = \frac{1}{r}\frac{\partial}{\partial r}\left(r \varepsilon D_p \frac{\partial c_p}{\partial r}\right) + \frac{\partial}{\partial z}\left(\varepsilon D_p \frac{\partial c_p}{\partial z}\right) - k_{\text{dep}} c_p, \tag{10}$$

$$\frac{\partial \varepsilon}{\partial t} = -\frac{\nu_{\text{dep}}}{\rho_{\text{dep}}} k_{\text{dep}} c_p. \tag{11}$$

Where: c_p – concentration of particulate matter in water [kg/m^3], D_p – diffucion coefficient of particles [m^2/s], k_{dep} – depolation coefficient [1/s], ν_{dep} – volume fraction of depolation [–], ρ_{dep} – density of settled particles [kg/m^3].

In this case, large particles (sand, clay) block the pores, thus reducing the filter's permeability. As a result, the flow decreases over time.

Boundary and initial conditions

The computational domain is an axisymmetric cylindrical domain

$$\Omega = \{(r, z) : 0 \leqslant r \leqslant R,\ 0 \leqslant z \leqslant H\}. \tag{12}$$

To close the system of equations (1)-(8), the following boundary and initial conditions are specified.

At the filter inlet ($z = 0$), a uniform axial flow of liquid and known concentrations of components are set:

$$\begin{cases} u_z(r, 0) = u_{in}, \\ u_r(r, 0) = 0, \\ c_i(r, 0) = c_{i,in},\ i = 1, \ldots, N. \end{cases} \tag{13}$$

Neumann's condition is used for pressure:

$$\left.\frac{\partial p}{\partial z}\right|_{z=0} = 0. \tag{14}$$

At the filter outlet ($z = H$), a fixed pressure is set, and for the remaining values, the conditions of zero longitudinal gradient are met:

$$\begin{cases} p(r, H) = p_{out}, \\ \left.\dfrac{\partial u_z}{\partial z}\right|_{z=H} = 0, \\ \left.\dfrac{\partial u_r}{\partial z}\right|_{z=H} = 0, \\ \left.\dfrac{\partial c_i}{\partial z}\right|_{z=H} = 0,\ i = 1, \ldots, N. \end{cases} \tag{15}$$

Axis of symmetry ($r = 0$): Due to the axisymmetric nature of the solution, the following conditions are satisfied:

$$\begin{cases} u_r(0, z) = 0, \\ \left.\dfrac{\partial u_z}{\partial r}\right|_{r=0} = 0, \\ \left.\dfrac{\partial p}{\partial r}\right|_{r=0} = 0, \\ \left.\dfrac{\partial c_i}{\partial r}\right|_{r=0} = 0,\ i = 1, \ldots, N. \end{cases} \tag{16}$$

Side surface of the filter ($r = R$): On the side wall of the filter, the adhesion conditions for the velocity and the absence of diffusion flow of substances are set:

$$\begin{cases} u_r(R, z) = 0, \\ u_z(R, z) = 0, \\ \left.\dfrac{\partial p}{\partial r}\right|_{r=0} = 0, \\ \left.\dfrac{\partial c_i}{\partial r}\right|_{r=R} = 0,\ \ i = 1, \ldots, N. \end{cases} \tag{17}$$

Neumann's condition is used for pressure:

$$\frac{\partial p}{\partial r}(R, z) = 0. \tag{18}$$

Initial conditions ($t = 0$):

For a non-stationary problem, the initial conditions are given in the form:

$$u_r(r, z, 0) = u_{r,0}(r, z),\ u_z(r, z, 0) = u_{z,0}(r, z),\ p(r, z, 0) = p_0(r, z), \tag{19}$$

$$\begin{cases} c_i(r, z, 0) = c_{i,0}, \\ q_i(r, z, 0) = 0,\ \ i = 1, \ldots, N, \\ \varepsilon(r, z, 0) = \varepsilon_0(r, z), \delta_c(r, z, 0) = 0. \end{cases} \tag{20}$$

The velocity and pressure fields are initialized by solving a stationary hydrodynamic problem.

3 Solution of the problem

For the numerical solution of the system of equations (1)-(8), the Finite Volume Method (FVM) is used, which ensures a strict balance of flows in each control volume and numerical stability when solving the conjugate problems of filtration and mass transfer.

3.1 Calculation grid and control volumes

The computational domain Ω is divided into a system of axisymmetric control volumes:

$$\Omega_{i,j} = \left[r_{i-\frac{1}{2}}, r_{i+\frac{1}{2}}\right] \times \left[z_{j-\frac{1}{2}}, z_{j+\frac{1}{2}}\right].$$

where

$$r_{i\pm\frac{1}{2}} = r_i \pm \frac{\Delta r}{2},\ \ z_{j\pm\frac{1}{2}} = z_j \pm \frac{\Delta z}{2}.$$

Volume of control volume:

$$V_{i,j} = 2\pi \int\limits_{r_{i-\frac{1}{2}}}^{r_{i+\frac{1}{2}}} r dr \int\limits_{z_{j-\frac{1}{2}}}^{z_{j+\frac{1}{2}}} dz = \pi \left(r_{i+\frac{1}{2}}^2 - r_{i-\frac{1}{2}}^2\right) \Delta z.$$

3.2 Discretization of the continuity equation

Integrating equation (1) over the control volume yields:

$$\sum_f (u \cdot n)_f S_f = 0,$$

$$f \in \{E,\ W,\ N,\ S\}.$$

where E – East face $\left(r_{i+1/2}, z_j\right)$, W – West face $\left(r_{i+1/2}, z_j\right)$, N – North face$\left(r_{i+1/2}, z_j\right)$, S – South face $\left(r_{i+1/2}, z_j\right)$.

In discrete form:

$$F^r_{i+\frac{1}{2},j} - F^r_{i-\frac{1}{2},j} + F^z_{i,j+\frac{1}{2}} - F^z_{i,j-\frac{1}{2}} = 0.$$

where the mass fluxes through the faces are defined as

$$F^r_{i+\frac{1}{2},j} = 2\pi r_{i+\frac{1}{2}} u_{r,i+\frac{1}{2},j} \Delta z,$$
$$F^z_{i,j+\frac{1}{2}} = \pi \left(r^2_{i+\frac{1}{2}} - r^2_{i-\frac{1}{2}} \right) u_{z,i,j+\frac{1}{2}}.$$

3.3 Discretization of momentum equations

Let's consider the axial component (similarly for the radial one).

Integrating (3) over V_i, j:

$$\sum_f \mu (\nabla u_z)_f \cdot n_f S_f - \frac{\mu}{k} u_{z,i,j} V_{i,j} - \left(\frac{\partial p}{\partial z} \right)_{i,j} V_{i,j} = 0.$$

Diffusion flux through the face $z_{j+\frac{1}{2}}$:

$$(\nabla u_z)_z \approx \frac{u_{z,i,j+1} - u_{z,i,j}}{\Delta z}.$$

The final discrete equation:

$$a_P u_{z,i,j} = a_N u_{z,i,j+1} + a_S u_{z,i,j-1} + a_E u_{z,i+1,j} + a_W u_{z,i-1,j} - (p_{i,j+1} - p_{i,j}) A_z.$$

where the coefficients are:

$$a_E = \mu \frac{S_E}{\Delta r},\ a_W = \mu \frac{S_W}{\Delta r},\ a_N = \mu \frac{S_N}{\Delta z},\ a_S = \mu \frac{S_S}{\Delta z}.$$

$$a_P = a_E + a_W + a_N + a_S + \frac{\mu}{\varkappa} V_{i,j}.$$

3.4 Pressure and speed correction

A pressure-based approach is used to link pressure and velocity fields.
Velocity correction:

$$u_z = u^*_z - d_z \frac{\partial p'}{\partial z},\ d_z = \frac{A_z}{a_P}.$$

Substituting into the continuity equation yields Poisson's equation for pressure correction:

$$a^{(p)}_P p'_{i,j} = a^{(p)}_E p'_{i+1,j} + a^{(p)}_W p'_{i-1,j} + a^{(p)}_N p'_{i,j+1} + a^{(p)}_S p'_{i,j-1} + b_{i,j}.$$

3.5 Discretization of the transport equations

Integration of (5) over the control volume yields:

$$\varepsilon \frac{c^{n+1}_{i,j} - c^n_{i,j}}{\Delta t} V_{i,j} + \sum_f F_f c_f = \sum_f D_{eff} S_f (\nabla c)_f - (r_{i,bulk} + a_s r_{i,surf}) V_{i,j}.$$

Convective currents are approximated by a counter-current scheme:

$$c_f = \begin{cases} c_P, & F_f > 0, \\ c_N, & F_f < 0. \end{cases}$$

Diffusion terms are approximated by a central differences.

3.6 Discretization of adsorption

Equation (6) is approximated by an implicit scheme:

$$\frac{q_i^{n+1} - q_i^n}{\Delta t} = k_f \left(q_i^* - q_i^{n+1}\right).$$

Where

$$q_i^{n+1} = \frac{q_i^n + k_f \Delta t q_i^*}{1 + k_f \Delta t}.$$

3.7 Conditions of convergence and stability

Convergence criterion

The iterative process is considered to have converged when the following conditions are met:

$$\frac{\sum\limits_{i,j} \left|\varphi_{i,j}^{k+1} - \varphi_{i,j}^{k}\right|}{\sum\limits_{i,j} \left|\varphi_{i,j}^{k+1}\right|} < \varepsilon_{tol}.$$

where $\varphi = \{u_r,\, u_z,\, p,\, c_i\}$, $\varepsilon_{tol} = 10^{-6}$.

Stability condition

For convective transport, the CFL constraint is satisfied:

$$CFL = \max\left(\frac{|u_r|\,\Delta t}{\Delta r}, \frac{|u_z|\,\Delta t}{\Delta z}\right) \leqslant 1.$$

Iterative Scheme:a n implicit iterative scheme with relaxation is used:

$$\varphi^{k+1} = \alpha \varphi_{new}^{k+1} + (1 - \alpha)\,\varphi^k,\ 0 < \alpha \leqslant 1.$$

4 Results and discussion

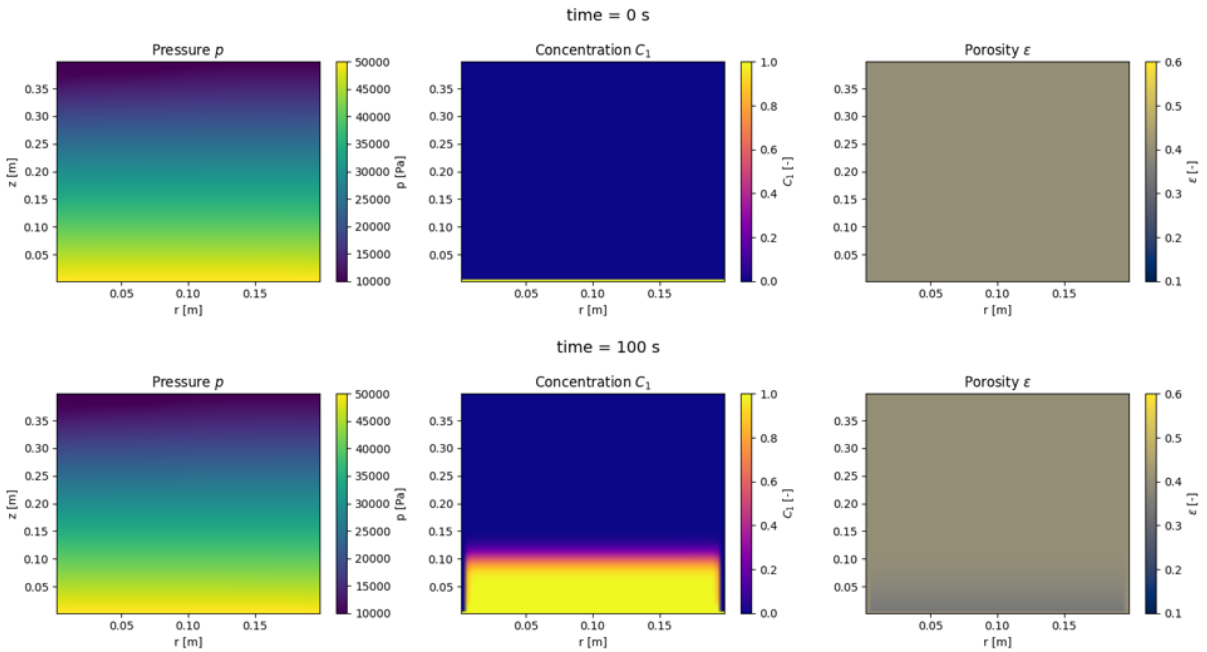

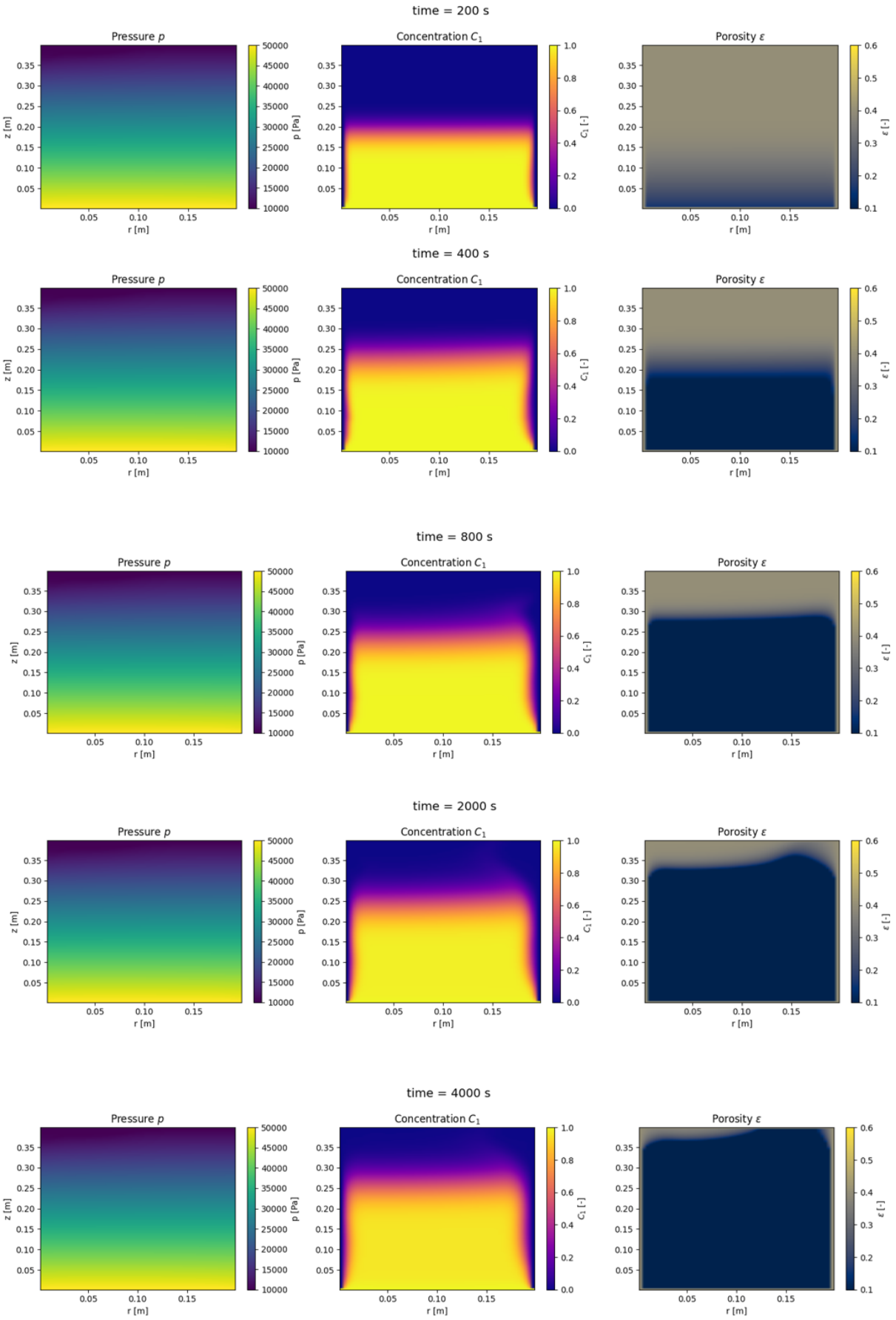
time = 200 s
Pressure p
Concentration C_1
Porosity ε
time = 400 s
Pressure p
Concentration C_1
Porosity ε
time = 800 s
Pressure p
Concentration C_1
Porosity ε
time = 2000 s
Pressure p
Concentration C_1
Porosity ε
time = 4000 s
Pressure p
Concentration C_1
Porosity ε
z [m]
r [m]
p [Pa]
C_1 [-]
ε [-]

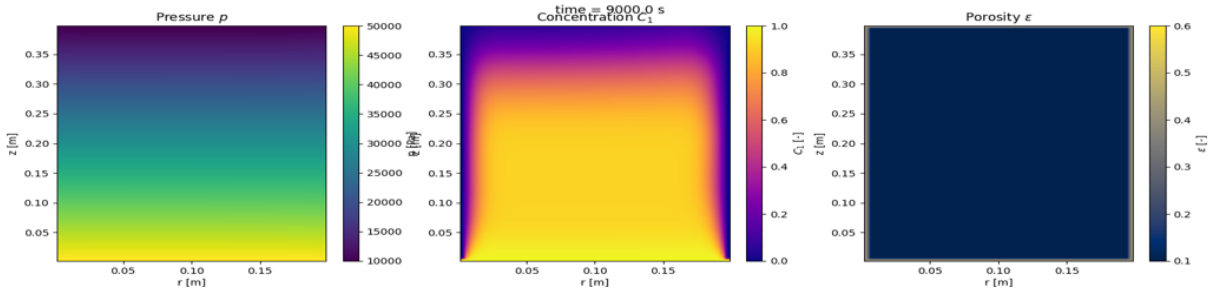

Figure 1 Temporal evolution of pressure field, normalized concentration, and porosity

Figure 1 illustrates the temporal evolution of pressure, normalized concentration, and porosity distributions in a cylindrical filter at different times. Initially, the pressure varies almost linearly along the filter axis, while the concentration is zero and the porosity is uniform, representing the clean filter state. As the fluid flows, a concentration front develops and propagates along the z-axis. In the lower part of the filter, increased concentration leads to a local reduction in porosity due to particle adsorption and accumulation. The front moves upward with a sharp concentration gradient, and porosity decreases precisely in the regions it passes through. Throughout the process, the pressure remains nearly linear, indicating that axial pressure gradients dominate the flow. Once the front reaches the filter top, the concentration approaches the inlet value, and the porosity at the bottom reaches its minimum, indicating filter saturation. Overall, the results highlight the strong coupling between fluid flow, solute transport, and porosity evolution.

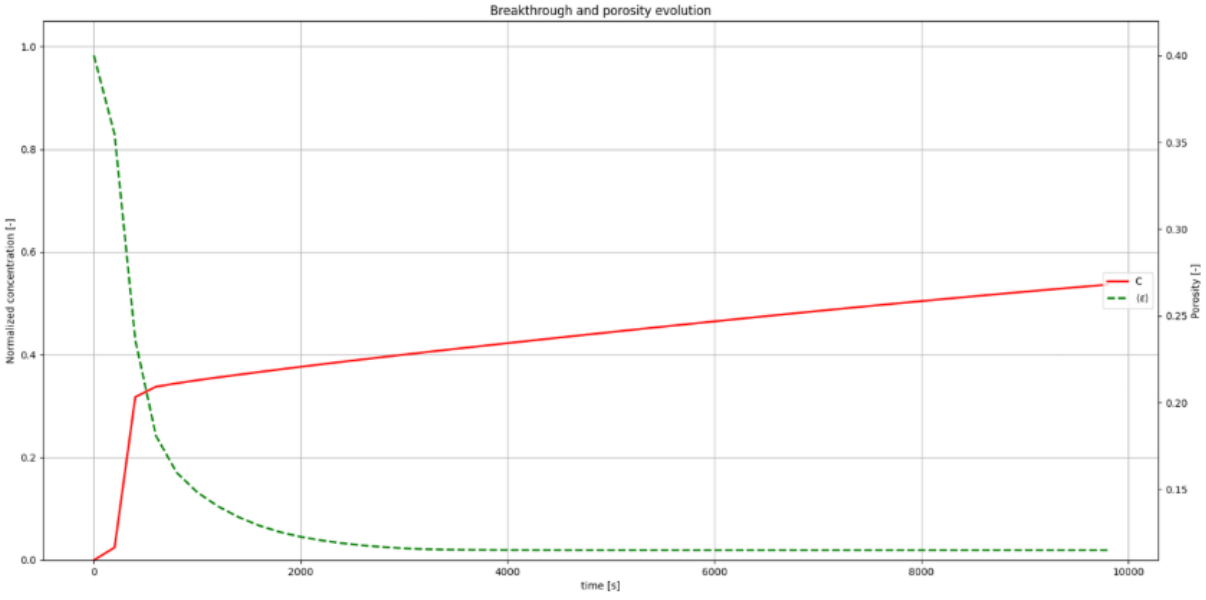

Figure 2 Time variation of normalized concentration and porosity at the point $z = H/2, r = 0$

Figure 2 shows the change in normalized concentration C_1 (–) and porosity ε (–) over time at the central point of the filter on the symmetry axis($r = 0$) at $z = H/2$. At the beginning, the concentration is zero and the porosity is uniform. As the liquid moves, the concentration increases sharply, and the porosity decreases due to adsorption and accumulation of the substance. The front is formed with a sharp drop in concentration, and porosity decreases precisely in the front zone. At later stages, the concentration

stabilizes and the porosity reaches a minimum value, indicating a formed deposit. In general, the graph demonstrates a direct relationship: an increase in concentration is accompanied by a decrease in porosity at a selected point in the filter.

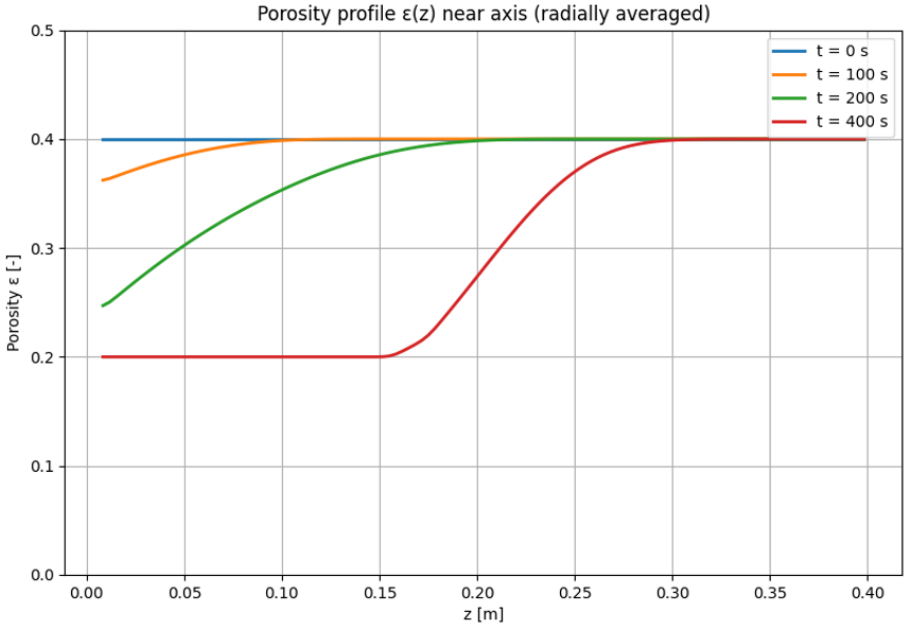

Figure 3 The change in porosity over time as the liquid moves along the z axis at $r = 0$ (on the axis of symmetry)

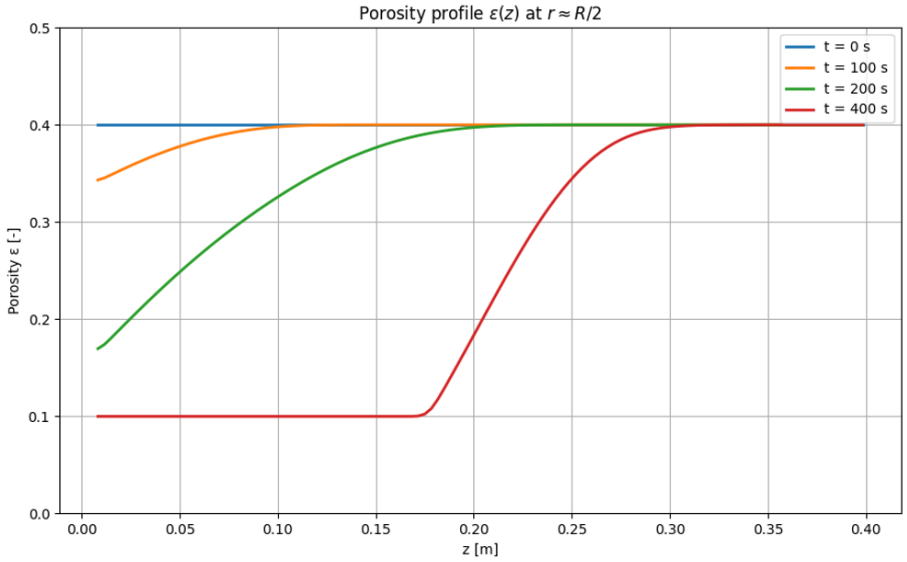

Figure 4 The change in porosity over time as the liquid moves along the z axis at $(r = R/2)$ (on the axis of symmetry)

Figure 3 shows the change in porosity ε (–) along the z-axis, on the axis of symmetry $(r = 0)$ in the filter. At the beginning of the process, the porosity is uniform along the entire axis, showing the initial state without deposition. By $t = 100$, an initial

deposition front is formed in the lower part of the filter($z \approx 0.05 - 0.10\,m$), where the porosity decreases noticeably, reflecting the local accumulation of matter.

At $t = 200$, the front moves up the axis $z \approx 0.2\,m$, the zone of minimum porosity expands, and the drop becomes sharper, which indicates active adsorption. By $t = 400$ the front reaches the middle part of the filter ($z \approx 0.17 - 0.3\,m$), the porosity in the front zone continues to decrease, forming a stable area with minimal values. In general, the graph demonstrates a direct relationship between the advance of the liquid front and the local decrease in porosity: the higher the front, the more it decreases along the filter axis.

Figure 4 shows the change in porosity ε (–) along the z axis, on the axis of symmetry in the filter($r = R/2$). At the beginning of the process, the porosity is uniform, similar to Fig. 3, showing the initial state without deposition. As the liquid moves, a deposition front forms, but compared to the center line (Fig. 3), the front at the half-radius develops more slowly.

Compared to Fig. 3 figure 4 shows that the radial displacement slows down the development of the front: the deposition front at the half-radius appears later and has a smoother profile, while on the axis the front is sharper and forms faster. This emphasizes the influence of radial flow inhomogeneity on the porosity distribution and demonstrates how the dynamics of deposition depends on the position in the filter - the front develops more intensely on the axis, and slower and more extended at the side wall.

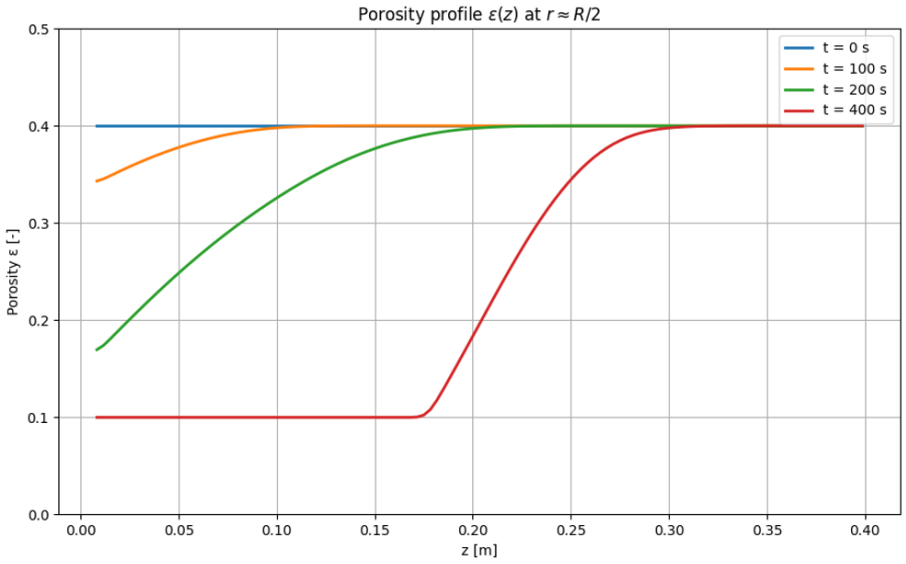

Figure 5 The change in porosity over time as the liquid moves along the z axis at $r = 0$ and $r = R/2$

Figure 5 shows a comparison of the change in porosity ε (–) along the z axis for two radial slices: $r = 0$ (solid line) and $r = R/2$ (dashed line) at several time steps. A comparison of the two lines clearly shows the influence of radial heterogeneity: on the axis the front is sharp and intense, while on the half-radius it develops more slowly and with less amplitude.

This figure emphasizes the connection between the radial positions in the filter and the dynamics of deposition: the closer to the axis, the faster the front forms and the more porosity decreases, while at the side wall the process is more extended and slower.

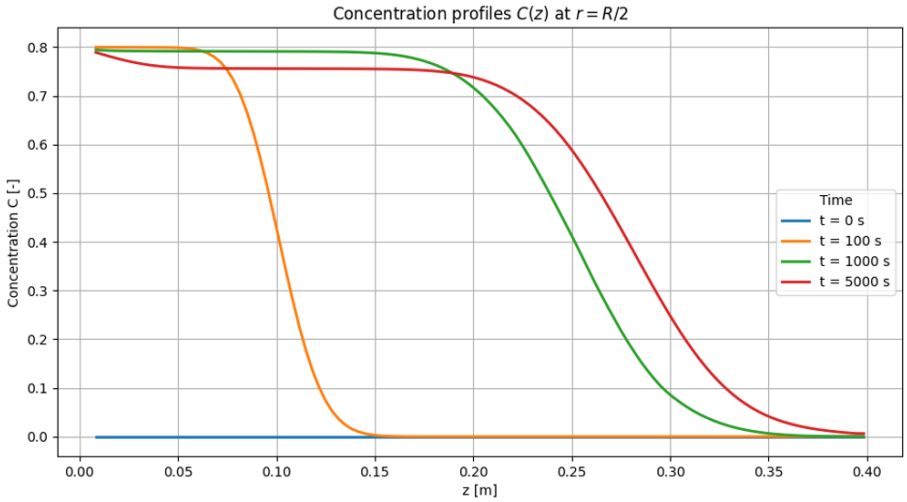

Figure 6 The change in concentration over time as the liquid moves along the z axis at $r = R/2$

Figure 6 shows the change in C_1 concentration along the z axis on a radial slice $r = R/2$ for several time steps. At the beginning of the process ($t = 0$), the concentration is almost zero along the entire axis, reflecting the initial state of the filter without penetration of the substance. At an early stage ($t = 100$), a concentration front forms in the lower part of the filter ($z \approx 0.05 - 0.15\,m$), where C_1 quickly increases to approximately 0.75–0.8.

At medium time steps (t=1000), the front moves higher along the ($z \approx 0.35m$), concentration increases in the front zone, but the front remains extended and less sharp than on the $r = 0$ axis, which reflects a slowdown in the flow at the side wall.

At the late stage ($t = 5000$), the front covers almost the entire length of the filter ($z \approx 0.35m$), the concentration stabilizes close to the input value, and the front remains extended, showing that the radial position affects the speed and shape of the movement of the substance: at the half-radius the front is slower and smoother than at the axis, where it is sharp and fast.

5 Conclusion

In this study, a coupled numerical model for filtration flow and solute transport in a cylindrical porous filter has been developed and implemented using the finite volume method. The hydrodynamic behavior of the flow was described by the axisymmetric Brinkman–Darcy equations, while mass transport was modeled using advection–diffusion equations with adsorption kinetics taken into account. The permeability of the porous medium was linked to porosity through the Kozeny–Carman relationship, allowing the evolution of the porous structure to be consistently incorporated into the model.

The numerical results demonstrate physically consistent pressure, concentration, and porosity fields and confirm the stability and conservation properties of the proposed finite volume discretization. The simulations show that the filtration process is primarily governed by the axial pressure gradient, while solute transport is controlled by the combined effects of convection, diffusion, and adsorption.

Over time, adsorption and particle deposition lead to a reduction in porosity, which decreases permeability and negatively affects filtration efficiency. The obtained results highlight the strong coupling between flow dynamics, mass transfer, adsorption processes, and porous structure evolution. The model is capable of capturing the transient behavior

of filter saturation and performance degradation, which is essential for the prediction of filter lifetime and operational efficiency.

Overall, the proposed approach provides a reliable and flexible numerical framework for analyzing filtration and transport processes in cylindrical porous media. It can be further extended to include more complex reaction mechanisms, non-Darcy flow regimes, or experimental validation, making it a useful tool for the design and optimization of filtration systems.

References

[1] Ravshanov N., Abdullaev Z., Khafizov O. Modeling the filtration of groundwater in multi-layer porous media // Construction of Unique Buildings and Structures – 2020. – Vol. 92. – Art. no. 9206.

[2] Ravshanov N., Turakulov J., Turkmanova S., Ungalov S. Numerical study of technological process of liquid solution filtration // AIP Conference Proceedings– 2025. – Vol. 3256. – Art. no. 040017. – doi: http://dx.doi.org/10.1063/5.0267147.

[3] Ravshanov N., Boborakhimov B.I., Berdiyorov Sh.Sh. Numerical modeling of liquid solution filtration in a cylindrical porous filter // Problems of Computational and Applied Mathematics. – 2025. – № 5(69). – doi: http://dx.doi.org/10.71310/pcam.5_69.2025.04.

[4] Bhattacharyya S., Dhinakaran S., Khalili A. Fluid motion around and through a porous cylinder // Chemical Engineering Science– 2006. – Vol. 61. – P. 4451-4461.

[5] Ghedira A., Lataoui Z., Benselama A.M., Bertin Y., Jemni A. Numerical simulation of incompressible two-phase flows with phase change process in porous media // Results in Engineering – 2025. – Vol. 25. – Art. no. 103706.

[6] Aydin A., Bilodeau C., Beckford C., Zhang G., Fattahpour H., et al. Modeling of drying process in porous media // Mathematics in Industry Reports (MIIR) .

[7] Amhalhel G.A., Furmanski P. Problems of modeling flow and heat transfer in porous media // Bulletin of the Institute of Thermal Technology of the Warsaw University of Technology. – 1997. – № 85.

[8] Puderbach V., Schmidt K., Antonyuk S. A coupled CFD-DEM model for resolved simulation of filter cake formation during solid-liquid separation // Processes– 2021. – Vol. 9. – Art. no. 826. – doi: http://dx.doi.org/10.3390/pr9050826.

[9] Starikovicius V. The multiphase flow and heat transfer in porous media // Reports from Fraunhofer ITWM . – 2003. – № 55.

[10] Zhang L., Guo B., Qin C., Xiong Y. A hybrid pore-network-continuum modeling framework for flow and transport in 3D digital images of porous media // Advances in Water Resources – 2024. – Vol. 190. – Art. no. 104753.

[11] Gahn M., Jäger W., Neuss-Radu M. Derivation of Stokes-Plate equations modeling fluid flow interaction with thin porous elastic layers // Preprint .

[12] Lavigne T., Suarez Afanador C.A., Obeidat A., Urcun S. Synthetic porous microstructures: Automatic design, simulation, and permeability analysis // Research Report

[13] Gu B., Sanaei P., Kondic L., Cummings L.J. Stochastic modeling of filtration with sieving in graded pore networks // Journal of Fluid Mechanics

[14] Chen Z., Liu S.Y., Christov I.C., Sanaei P. Flow and fouling in elastic membrane filters with hierarchical branching pore morphology // Physics of Fluids – 2021. – Vol. 33. – Art. no. 062009. – doi: http://dx.doi.org/10.1063/5.0054637.

[15] Koka R., Ganjikunta A. Effect of the aligned magnetic field over a stretching sheet through porous media in Casson fluid flow // CFD Letters. – ISSN 2180-1363.

[16] Vecherkovskaya A., Popereshnyak S. Mathematical modeling of the process of fluid filtration through a multi-layer filtering element // *Technology Audit and Production Reserves*. – 2017. – doi: http://dx.doi.org/10.15587/2312-8372.2017.109309.

[17] Girelli A., Giantesio G., Musesti A., Penta R. Multiscale computational analysis of the steady fluid flow through a lymph node // *Biomechanics and Modeling in Mechanobiology*. – 2024. – Vol. 23. – P. 2005-2023. – doi: http://dx.doi.org/10.1007/s10237-024-01879-7.

[18] Zhu T. Unsteady porous-media flows. – 2016. – https://mediatum.ub.tum.de/doc/1279870/1279870.pdf.

УДК 519.6+51-74::628.395

ЧИСЛЕННОЕ МОДЕЛИРОВАНИЕ ПРОЦЕССОВ ФИЛЬТРАЦИИ И ТРАНСПОРТА В ЦИЛИНДРИЧЕСКОМ ПОРИСТОМ ФИЛЬТРЕ С ИСПОЛЬЗОВАНИЕМ МЕТОДА КОНЕЧНЫХ ОБЪЕМОВ

Равшанов Н.,* *Боборахимов Б.И., Бердиёров Ш.Ш.

*uzbekpy@gmail.com

Научно-исследовательский институт развития цифровых технологий и искусственного интеллекта,

100125, Узбекистан, г. Ташкент, Мирзо-Улугбекский р-он, м-в Буз-2, д. 17А.

В данной работе исследуется численное моделирование потока при фильтрации и переносе растворенных компонентов в цилиндрической пористой среде. Математическая формулировка основана на осесимметричных уравнениях Бринкмана-Дарси, описывающих гидродинамические процессы, а также на системе уравнений конвективно-диффузионного переноса с учетом адсорбции на твердой матрице. Проницаемость пористой среды задается с помощью модели Козени-Кармана. Численное решение реализовано с использованием метода конечных объемов, что гарантирует выполнение законов сохранения в каждом контрольном объеме. Разработан вычислительный алгоритм для определения распределения давления, скоростей и концентраций компонентов. Изучено влияние параметров пористой структуры и характеристик кинетики адсорбции на эффективность и характеристики процесса фильтрования.

Ключевые слова: цилиндрическая пористая среда, фильтрация, перенос вещества, модель Бринкмана–Дарси, адсорбция, метод конечных объемов, численное моделирование.

Цитирование: *Равшанов Н., Боборахимов Б.И., Бердиёров Ш.Ш.* Численное моделирование процессов фильтрации и транспорта в цилиндрическом пористом фильтре с использованием метода конечных объемов // Проблемы вычислительной и прикладной математики. – 2026. – № 1(71). – С. 28-42.

DOI: https://doi.org/10.71310/pcam.1_71.2026.03

№ 1(71) 2026

ISSN 2181-8460

HISOBLASH VA AMALIY MATEMATIKA MUAMMOLARI

ПРОБЛЕМЫ ВЫЧИСЛИТЕЛЬНОЙ И ПРИКЛАДНОЙ МАТЕМАТИКИ

PROBLEMS OF COMPUTATIONAL AND APPLIED MATHEMATICS

RAQAMLI TEXNOLOGIYALAR VA
SUN'IY INTELLEKTNI RIVOJLANTIRISH
ILMIY-TADQIQOT INSTITUTI

ПРОБЛЕМЫ ВЫЧИСЛИТЕЛЬНОЙ И ПРИКЛАДНОЙ МАТЕМАТИКИ

№ 1(71) 2026

Журнал основан в 2015 году.
Издается 6 раз в год.

Учредитель:
Научно-исследовательский институт развития цифровых технологий и искусственного интеллекта.

Журнал зарегистрирован в Агентстве информации и массовых коммуникаций при Администрации Президента Республики Узбекистан.
Свидетельство №0856 от 5 августа 2015 года.

ISSN 2181-8460, eISSN 2181-046X

Адрес редакции:
100125, г. Ташкент, м-в. Буз-2, 17А.
Тел.: +(998) 71 263-41-98.
Э-почта: journals@airi.uz.
Веб-сайт: https://journals.airi.uz.

Дизайн и вёрстка:
Шарипов Х.Д.

Отпечатано в типографии НИИ РЦТИИ.
Подписано в печать 25.02.2026 г.
Формат 60x84 1/8. Заказ №1. Тираж 100 экз.

PROBLEMS OF COMPUTATIONAL AND APPLIED MATHEMATICS

No. 1(71) 2026

The journal was established in 2015.
6 issues are published per year.

Founder:
Digital Technologies and Artificial Intelligence Development Research Institute.

The journal is registered by Agency of Information and Mass Communications under the Administration of the President of the Republic of Uzbekistan.
Certificate of Registration No. 0856 of 5 August 2015.

ISSN 2181-8460, eISSN 2181-046X

Address:
100125, Tashkent, Buz-2, 17A.
Tel.: +(998) 71 263-41-98.
E-mail: journals@airi.uz.
Web-site: https://journals.airi.uz.

Layout design:
Sharipov Kh.D.

DTAIRI printing office.
Signed for print 25.02.2026
Format 60x84 1/8. Order No. 1. Print run of 100 copies.

Содержание

Contents